ELSEVIER

Polymer 43 (2002) 4923–4933

polymer

www.elsevier.com/locate/polymer

Structure of blown film from blends of polyethylene and high melt strength polypropylene

A.C. Chang[a], L. Tau[b], A. Hiltner[a,*], E. Baer[a]

[a]*Department of Macromolecular Science, Center for Applied Polymer Research, Case Western Reserve University, 10900 Euclid Avenue, Cleveland, OH 44106-7202, USA*

[b]*Polyolefins and Elastomers R & D, The Dow Chemical Company, Freeport, TX 77541, USA*

Received 23 January 2002; received in revised form 25 April 2002; accepted 29 April 2002

Abstract

The structure of blown film processed from linear low density polyethylene blended with up to 30 wt% of a high melt strength polypropylene (hmsPP) was examined using primarily atomic force microscopy and wide angle X-ray scattering. The study focused on two polyethylene resins with the same density: a conventional Ziegler–Natta catalyzed linear low density polyethylene (znPE) and a blend of a Ziegler–Natta catalyzed and a metallocene catalyzed linear low density polyethylene (zn/mPE). Parallel characterization was performed on blown film of the hmsPP and blown film of each of the polyethylene resins. In films of the blends, the hmsPP was well-dispersed in the polyethylene matrix as elongated domains. In the domains, the hmsPP crystallized as planar row-nucleated structures with the long axis of the lamellae perpendicular to the extrusion direction. Row-nucleated hmsPP lamellae provided a template for epitaxial crystallization of polyethylene lamellae. The 42° angle of the lattice match imparted a characteristic herringbone texture to the polyethylene. Blending with hmsPP increased the tensile modulus and strength of polyethylene film without significantly affecting the ultimate elongation.

Keywords: High melt strength polypropylene; Polyethylene; Polyethylene/polypropylene blends

1. Introduction

Despite the advantages of higher stiffness and higher heat resistance that polypropylene could bring to films, compared to polyethylene, poor melt strength and bubble instability of traditional polypropylene resins have prevented their use in blown film processes. Consequently, production of biaxially oriented polypropylene film has been limited largely to methods that orient film in the solid state, as in tentering where the extrudate is quenched, reheated, and oriented into film [1]. It is apparent that opportunities exist for a high melt strength polypropylene (hmsPP) resin in blown film, extrusion foaming and thermoforming processes.

Previous efforts to obtain polypropylene resins with superior melt strength focused on introduction of long chain branching [2,3], as a means of reinforcing the entanglement network in the melt [4,5]. hmsPP resins introduced recently provide significantly enhanced processability compared to conventional resins without sacrificing physical properties [6].

Combining hmsPP with ethylene polymers overcomes some of the limitations typical of polypropylene resins. Blending hmsPP with polyethylene enhances stiffness and tensile strength of inherently tough and tear resistant polyethylene blown film. Good compatibility of hmsPP with ethylene polymers in blown monolayer film of blends or coextruded multilayers provides for an optimum balance of properties [7]. Epitaxial crystallization of polyethylene on oriented polypropylene substrates imparts exceptionally strong adhesion [8,9]. As a consequence, polyethylene/polypropylene films containing ultra-thin layers of epitaxially crystallized polyethylene exhibit a synergistic increase in mechanical properties [10,11].

The specific property balance achieved in polyethylene/propylene films derives from the oriented morphology achieved in the film process. The present study focuses on characterizing the morphology of blown film obtained from blends of polyethylene with up to 30 wt% of hmsPP. The oriented phase morphology is subsequently correlated with tensile properties.

* Corresponding author. Tel.: +1-216-368-4186; fax: +1-216-368-6329.
E-mail address: pah6@po.cwry.edu (A. Hiltner).

0032-3861/01/$ - see front matter
PII: S0032-3861(02)00304-X

Table 1
Film density

PP (wt%)	Density (g cm^{-3})	
	50 μm film	20 μm film
hmsPP/znPE		
0	0.9187 ± 0.0001	0.9181 ± 0.0001
10	0.9170	0.9157
20	0.9153	0.9135
30	0.9134	0.9115
100	0.9019	0.9014
hmsPP/(zn/mPE)		
0	0.9144 ± 0.0001	0.9125 ± 0.0001
10	0.9131	0.9114
20	0.9117	0.9099
30	0.9104	0.9084
100	0.9019	0.9014

2. Experimental

A hmsPP, two linear low density polyethylenes, and blends of the polypropylene with each of the polyethylenes were provided in the form of 20 μm (0.8 mil) and 50 μm (2.0 mil) blown film by The Dow Chemical Company. The films were processed under identical conditions except that the take-off speed was increased to obtain the thinner film. The hmsPP was also provided as pellets. As indicated by the manufacturer, the hmsPP was a modified impact resin with 16 wt% of an ethylene–propylene rubber (EPR) and melt flow index 0.35 g/10 min. One polyethylene was a Ziegler–Natta catalyzed ethylene–octene copolymer (znPE) with density 0.920 g cm^{-3} and melt flow index 1.0 g/10 min. The other polyethylene was a blend (zn/mPE) with density 0.916 g cm^{-3} that consisted of 63 wt% of a Ziegler–Natta catalyzed ethylene–octene copolymer ($\rho = 0.925$ g cm^{-3}) and 37 wt% of a metallocene catalyzed ethylene–octene copolymer ($\rho = 0.902$ g cm^{-3}), the blend had melt flow index 1.0 g/10 min. The melt flow index was measured with a load of 2.16 kg at 190 °C for polyethylene and at 230 °C for polypropylene.

Density of the blown film was measured using an isopropanol–water density gradient column calibrated with glass floats according to ASTM D1505-85. Specimens were allowed to equilibrate in the column for 3 h before a measurement was taken. The 20 μm film had slightly lower density, hence slightly lower crystallinity, than the 50 μm film of the same composition as a result of faster cooling, Table 1. Also, films with zn/mPE had lower density than the corresponding films with znPE.

To reveal the morphology in the machine or extrusion direction (MD) and in the transverse or blow-up direction (TD), pieces of film were sandwiched between two sheets of partially cured embedding media (SPI-PON 812) from Structure Probe Incorporated and allowed to cure at 75 °C for 10 h under light pressure. Partial curing prevented diffusion of the embedding media into the films. The embedded specimens were trimmed with a diamond band saw, polished, and microtomed with a glass knife at a sample temperature of −50 °C and knife temperature of −40 °C with a cutting rate of 2 mm s^{-1}.

To reveal the morphology normal to the film surface (ND), films were etched with a 0.7 wt% solution of potassium permanganate in a 2:1 (v/v) mixture of concentrated sulfuric acid and 85% orthophosphoric acid [12]. Specimens were etched for 2–4 h until the thickness was reduced by 40–60%. Etching preferentially removed the amorphous phase thereby revealing the lamellar morphology. Etched and microtomed specimens were rinsed with methanol and blown dry with compressed air.

Atomic force microscopy (AFM) images were obtained in air with a Digital Instruments Nanoscope IIIa AFM in the tapping mode. Hard tapping at 50% or less of the free oscillation amplitude (A_0) with driving amplitudes of 250–350 mV was used to bring out differences in modulus between polypropylene and polyethylene. Lighter tapping at 75% A_0 with driving amplitudes of 75–150 mV was used for etched specimens for high definition of the lamellar texture.

Pellets of hmsPP were compression molded at 230 °C and microtomed for examination in the AFM. In addition, the microtomed surfaces were etched with 1,1,2,2-tetrachloroethane at 80 °C for 5 h [13], coated with 100 Å of gold and examined with a scanning electron microscope.

Wide angle X-ray scattering (WAXS) flat film patterns from the films were obtained with a Philips PW1830 X-ray source fitted with a Statton camera. For ND patterns, pieces of film were assembled into a stack about 0.5 mm thick. For MD and TD patterns, film stacks were embedded in epoxy and sections with the desired orientation were cut with a low speed diamond saw.

Tensile specimens with the ASTM 1708 microtensile dog bone geometry were cut from the films in the MD and the TD. Thickness was obtained by dividing the weight of the specimen by its density and surface area. Tensile stress–strain measurements were conducted in an Instron machine using a nominal strain rate of 100% min^{-1}. The natural draw ratio λ_n was taken from the engineering strain at the onset of strain hardening ε_{onset}, and was calculated as $\lambda_n = (\varepsilon_{onset}/100) + 1$.

3. Results and discussion

3.1. High melt strength polypropylene

The hmsPP used in this study contained about 16 wt% EPR synthesized in a secondary step following propylene polymerization. Typically, EPR made in this manner contains chains of variable composition with a distribution of ethylene and propylene sequence lengths [14,15]. The sequence lengths can include noncrystallizable short blocks and runs that are long enough to crystallize as lamellae. As a

consequence, the heterogeneous solid-state structure may be complex [16,17].

An AFM phase image of hmsPP is shown in Fig. 1(a). This technique shows relative differences in modulus with lighter shades indicating higher modulus and darker shades representing lower modulus. The soft EPR phase appears as dark particles 1 μm or smaller in diameter dispersed in the lighter polypropylene matrix. Area analysis of lower magnification images confirms the 16 wt% EPR formulation. The horizontal lines and the occasional vertical streak in the images are artifacts of microtoming.

Many of the EPR particles are heterogeneous consisting of a hard core surrounded by a soft shell. Considering the varied chemical species that comprise EPR, it is assumed that the soft shell consists of noncrystallizable chains and that the core contains crystallizable chains. Examination of the core reveals a granular texture that suggests an aggregate of hard, crystalline subparticles bound together by a softer, amorphous phase. Other EPR particles are uniformly dark indicating an amorphous composition of noncrystallizable chains. These particles could also be slices through the amorphous shell of heterogeneous particles.

Etching hmsPP with 1,1,2,2-tetrachloroethane removed the amorphous fractions of EPR. Small cavities in Fig. 1(b) correspond to complete removal of the homogeneous particles. The larger cavities sometimes contain material that is not removed by etching. Eliminating the amorphous fractions from the heterogeneous particles reveals the crystalline core and sometimes fibrils connecting the crystalline core to the polypropylene matrix. The etch-resistant fibrils possibly consist of chains with long ethylene and propylene sequences that are anchored by cocrystallization in both the polypropylene matrix and the crystalline EPR core.

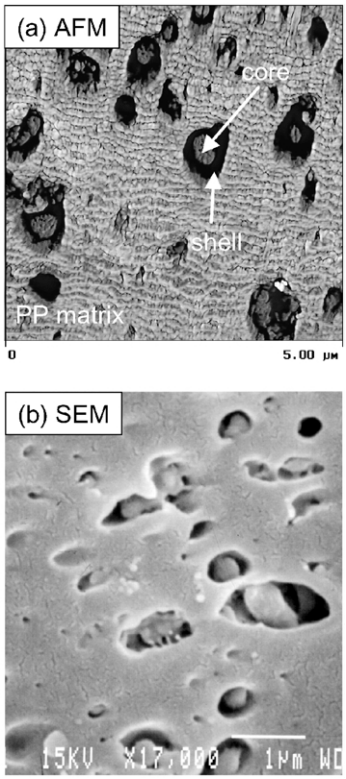

Fig. 1. High melt strength polypropylene, compression molded. (a) AFM phase image with hard tapping, and (b) scanning electron micrograph after removing the amorphous EPR fractions by etching with 1,1,2,2-tetrachloroethane.

3.2. High melt strength polypropylene film

The oriented structure of hmsPP blown film is revealed in AFM phase images of cross-sections microtomed parallel (MD) and perpendicular (TD) to the extrusion direction. In the MD view of the 20 μm film, the softer EPR phase is visible as large elongated domains and as very thin dark streaks aligned in the extrusion direction, Fig. 2(a). The large particles contain hard granular subparticles of crystallizable EPR, whereas the elongated rods appear to consist of only soft amorphous material. The corresponding TD image shows circular EPR domains that are cross-sections of the large domains detected in the MD view, and some small dark flecks that could be cross-sections of the dark streaks in the MD view, Fig. 2(b). Combined, the images suggest that the EPR phase is present in hmsPP film as large elongated particles that contain the crystalline fractions and as long thin rods that consist of amorphous chains. In 50 μm film, produced at a lower take-off rate, the large particles are closer to spherical and the rods are less elongated than in 20 μm film.

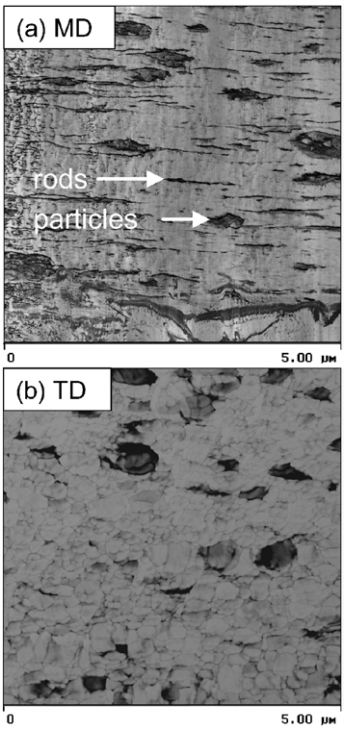

Fig. 2. AFM phase images of 20 μm hmsPP blown film with hard tapping. (a) Machine direction (MD), and (b) transverse direction (TD).

The low extension ratio of large, composite EPR particles compared to the high extension of amorphous rods arises from the presence of higher molecular weight crystallizable EPR fractions [14] and the possibility for grafting and/or cross-linking of these fractions in hmsPP [18–20]. The composite EPR particles in blown film appear smaller with less rubbery material than the composite EPR particles of the unoriented material (compare Fig. 2(a) with Fig. 1(a)). Possibly, amorphous EPR chains separate from the composite particles and elongate into rods under the extensional flow during processing. Additionally, rods can originate from elongation and possibly breakup of small domains of amorphous EPR fractions that are present in the unoriented material.

Etching into the interior allows access to the bulk morphology in the plane of the film (ND). The time used for acid etching typically reduces film thickness by 40–60%. Etching preferentially removes the amorphous EPR fractions. Careful examination of the corresponding height images (not shown) reveals depressions of the appropriate size and shape, where EPR particles had been. Often the larger depressions contain granular particles of the more slowly etched crystalline EPR fractions, as in the example indicated by an arrow in Fig. 3(a). Although the etching solution removes both crystalline and amorphous phases, faster etching of the amorphous phase reveals the lamellar texture of hmsPP for imaging by AFM. Images of 20 μm hmsPP film show irregular stacks of lamellae with the long axis of the lamellae perpendicular to the MD, Fig. 3(a). The lamellae are arranged edge-on with no apparent twisting about the lamellar axis. Considering that lamellar growth occurs in the direction of the long axis, it would appear that the lamellae in a column originate from a common nucleus such as a fibrous crystal. Very light etching reveals longer stacked lamellae close to the inner film surface, Fig. 3(b). This is consistent with the higher temperature inside the bubble and therefore a somewhat slower crystallization rate at the inner surface. Regardless, the columnar arrangement appears to persist through the thickness of the film.

A few thinner lamellae, oriented almost parallel to the extrusion direction and perpendicular to the stacked lamellae, are visible in the AFM images. Examples are easily seen in the lower left quadrant of Fig. 3(a); however, they are more numerous in images of lightly etched films, as in Fig. 3(b). These may constitute a second lamellar population that nucleates by crystallographic branching from the (010) plane of individual lamellae in the column [21–23]. In spherulites, this type of epitaxial growth produces the characteristic lamellar texture of polypropylene commonly known as cross-hatching.

The WAXS patterns in the ND and TD of 20 μm hmsPP film are identical, and reveal three strong equatorial reflections corresponding to the (110), (040), and (130) planes of the polypropylene α-form, Fig. 4(a) and (b). The presence of some β-form crystals is indicated by an equatorial reflection corresponding to the (110) plane. The equatorial location of the ND and TD *hk*0 reflections suggests *c*-axis orientation in the MD. The corresponding MD pattern reveals the *hk*0 reflections as rings of equal

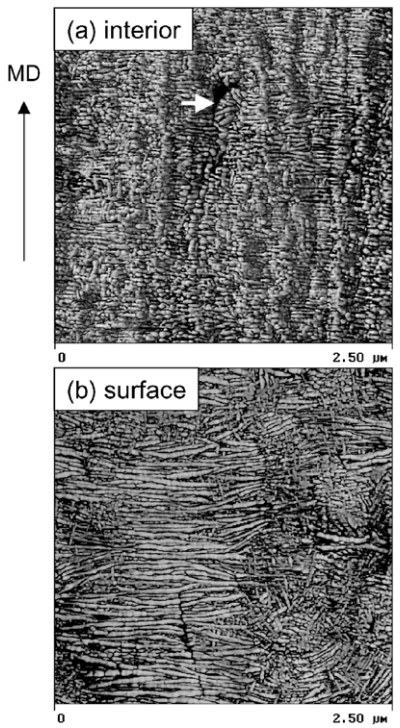

Fig. 3. AFM phase images of 20 μm hmsPP blown film in the normal direction (ND) after etching, with light tapping. (a) Near the center, and (b) near the inner surface.

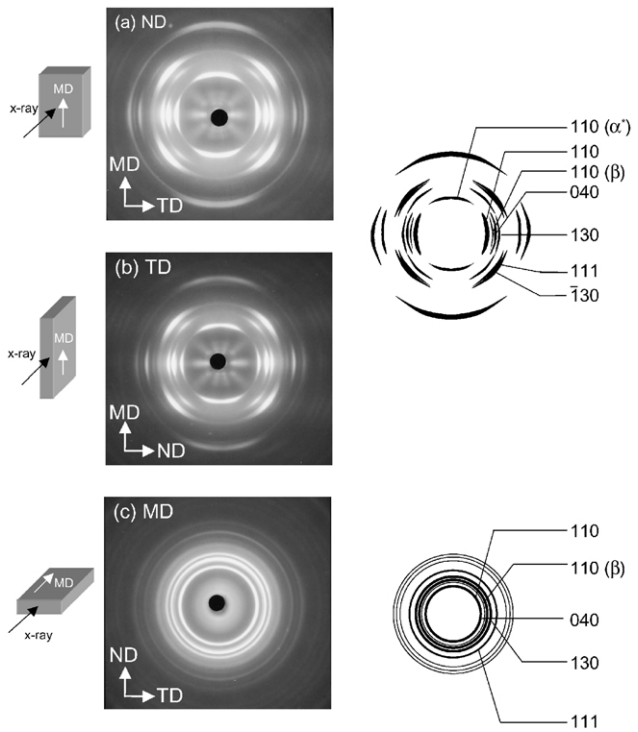

Fig. 4. WAXS patterns from the three orthogonal directions of 20 μm hmsPP film: (a) ND, (b) TD, and (c) MD.

intensity at all azimuths, Fig. 4(c). A row-nucleated structure with axial symmetry of the radial lamellae about the MD provides the distribution of scattering sites necessary to produce such patterns. Indeed, WAXS patterns identical to those in Fig. 4(a) and (b) obtained with the beam perpendicular to the MD and at angles intermediate between the ND and TD corroborate this interpretation. Identification of higher levels of symmetry would require construction of X-ray pole figures [24]. An additional 110 reflection appears on the meridian with intensity maxima at azimuthal angles of $\pm 20°$ (a^*-axis orientation). This reflection is attributed to epitaxially crystallized lamellae with lamellar axis almost parallel to the MD (Fig. 3) [22].

The row-nucleated columnar structure is not observed in conventional polypropylene film oriented from the solid state [25]. Rather, it resembles the row-nucleated structures produced by melt orientation of high density polyethylene that are identified as shish–kebabs [26–29]. These structures require the presence of extended-chain fibrillar crystals (shish) that serve to nucleate regular lamellar crystallization (kebabs). It is possible that the grafting reactions used in the production of a hmsPP result in a population of high molecular weight chains that do not have time to relax from the oriented melt before the onset of crystallization. These fibrous crystals serve as extended chain nuclei for lamellar growth.

WAXS patterns identical to those in Fig. 4, with mixed c-axis and a^*-axis orientation, are obtained in another instance where the melt crystallizes under a high shear stress [30,31]. This is in the skin layer of injection molded polypropylene. Here, interpretation of the WAXS also leads to the shish–kebab structure with fibrous crystals forming the nuclei for c-axis oriented growth. The analogy extends to identification of small lamellae with a^*-axis orientation epitaxially crystallized on the kebabs.

3.3. Polyethylene film

Phase images of 20 μm polyethylene blown film reveal densely packed, curving lamellae of znPE and zn/mPE, Fig. 5(a) and (b). It is not easy to discern any preferential orientation of the lamellar axis in these images.

The WAXS patterns of znPE film in the ND and TD yield broad arcs, whereas the MD pattern shows no orientation, Fig. 6. The reflections correspond to the (110), (200), (210) and (020) planes of the orthorhombic form of polyethylene [32–34]. Arcs in the ND and TD patterns suggest some mild orientation in the MD. However, the breadth of the arcs is totally consistent with the absence of row-nucleated polyethylene shish–kebabs or other morphology with well-defined lamellar orientation. The 20 μm zn/mPE film produces the same diffraction patterns as shown in Fig. 6.

3.4. Phase morphology of blend films

Blown films fabricated from blends have hmsPP as the

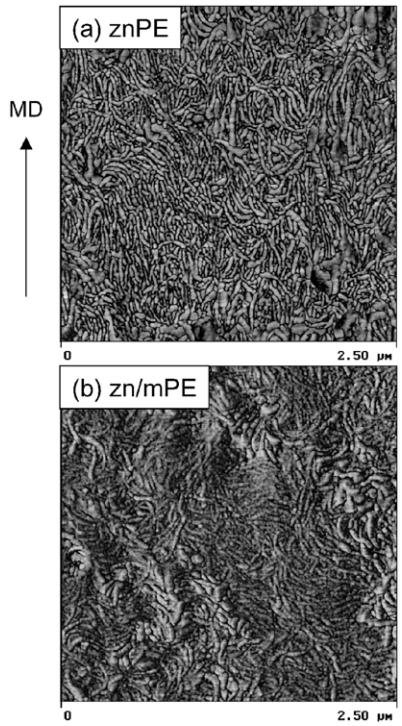

Fig. 5. AFM phase images of 20 μm polyethylene blown film in the normal direction (ND) after etching, with light tapping: (a) znPE film and (b) zn/mPE film.

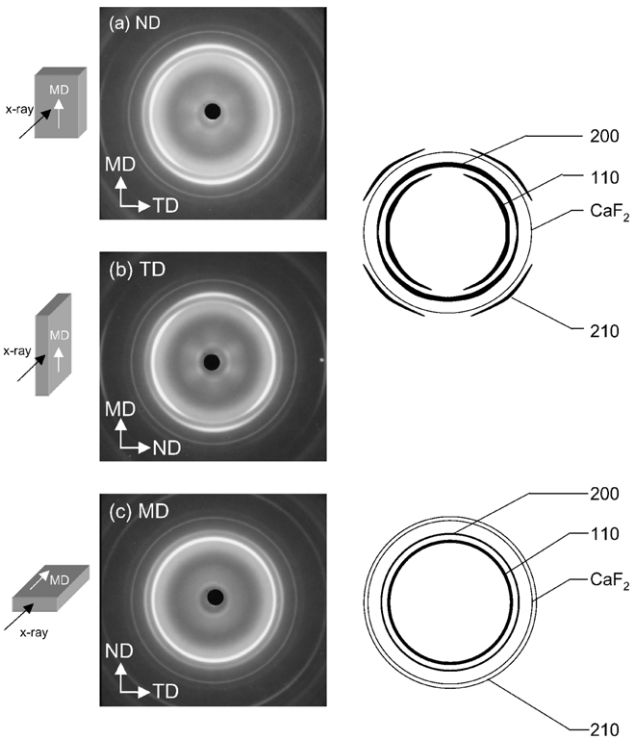

Fig. 6. WAXS patterns from the three orthogonal directions of 20 μm znPE blown film: (a) ND, (b) TD, and (c) MD.

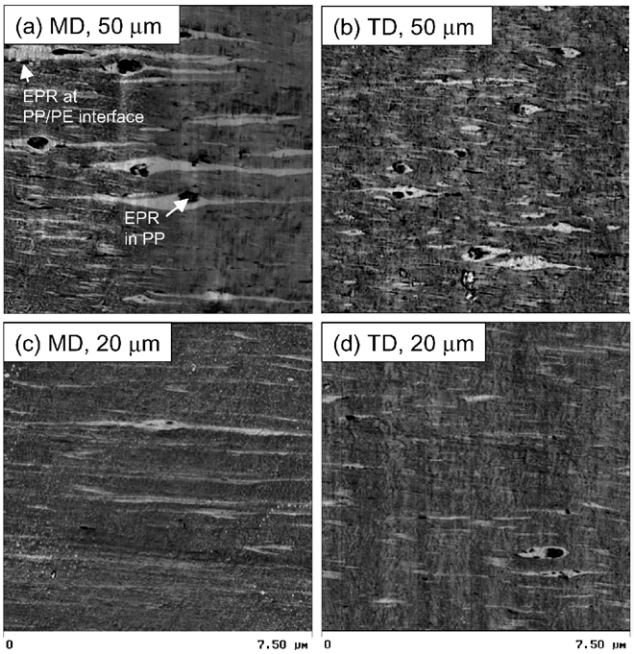

Fig. 7. AFM phase images of 10/90 hmsPP/znPE blown film with moderately hard tapping. (a) MD of 50 μm film, (b) TD of 50 μm film, (c) MD of 20 μm film, and (d) TD of 20 μm film.

minor constituent (10–30 wt%) and either znPE or zn/mPE as the major constituent. An AFM image of the MD cross-section of 50 μm 10/90 hmsPP/znPE film shows the phase morphology of the immiscible constituents, Fig. 7(a). The lighter (i.e. harder) hmsPP domains are dispersed in the darker (i.e. softer) znPE matrix. The hmsPP domains are elongated in the MD. The corresponding image of the TD cross-section shows the hmsPP domains to be about half as wide as they are long, Fig. 7(b). Composite EPR particles remain in the hmsPP phase, perhaps attached by the fibrils seen in Fig. 1(b). Domains that contain composite EPR particles bulge around the undeformed particle and then taper off towards the edges. Often the taper is longer and thinner in the process direction (the right side of the domains in Fig. 7(a)) than in the wake of the composite EPR particle. The EPR particle may shield hmsPP from elongational forces during processing resulting in lower deformation. Occasionally, a very dark, elongated particle appears at the hmsPP/znPE interface. Amorphous EPR fractions are probably mobile enough to migrate from the hmsPP phase.

In 20 μm film, the hmsPP domains are longer and thinner than in 50 μm film, Fig. 7(c) and (d). Examination of hmsPP domains in lower magnification images shows them to be about twice as long in 20 μm film as in 50 μm film. The dimensional difference is consistent with the approximate doubling of the take-off speed of 20 μm film. The TD cross-sections of hmsPP domains in 20 and 50 μm film are about the same width (compare Fig. 7(d) with (b)). This is consistent with the constant blowup ratio used to prepare both film thicknesses. Although the corresponding reduction in thickness puts the domain size at the nanoscale, about 30 nm, the high melt strength of hmsPP prevents domain breakup. Only a few dark areas of amorphous EPR are visible in images of 20 μm film. It is possible that amorphous EPR forms a surface layer on the very thin films in much the same way that lower molecular weight, higher branch content fractions of linear low density polyethylene form an amorphous surface layer on blown film [35,36].

It is convenient to describe the hmsPP domains in blend films as tapered planks (50 μm film) or ribbons (20 μm film) aligned with the long axis in the MD. This is represented schematically in Fig. 8(a) and (b). Differences in the dimensions of the domains in 50 and 20 μm film parallel differences in the macroscopic deformation in the blown film process. Thus, the ribbons in 20 μm film have about the same width but about twice the length and half the thickness of the planks in 50 μm film. The schematic includes amorphous EPR fractions that occasionally appear at the phase boundary as very small, elongated particles. Increasing hmsPP content to 20 and 30 wt% increases the concentration of hmsPP domains without significantly altering their size and shape. Furthermore, changing the matrix from znPE to zn/mPE has no effect on the hmsPP domain morphology.

3.5. Lamellar morphology of blend films

The AFM images in Fig. 9 show two regions of 20 μm 10/90 hmsPP/znPE blown film. In Fig. 9(a), the lamellar morphology of the znPE matrix in regions removed from a hmsPP domain resembles the morphology of znPE film with

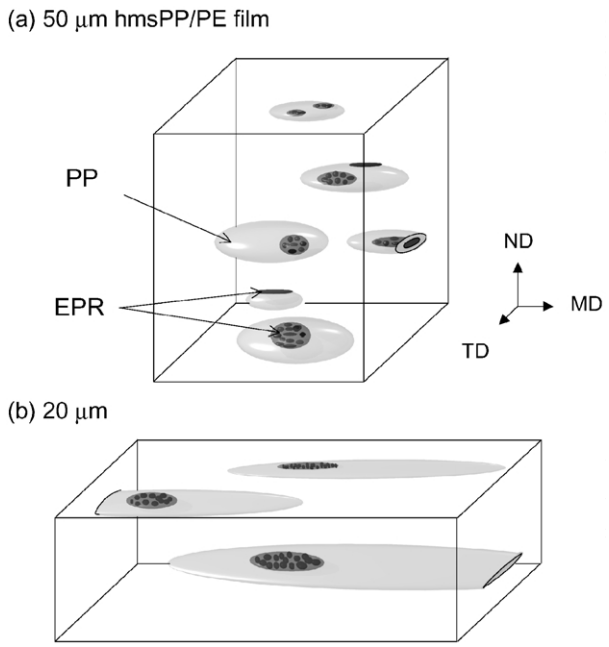

Fig. 8. Schematic representations of the phase morphology in hmsPP/znPE and hmsPP/(zn/m)PE blown film. (a) 50 μm film and (b) 20 μm film.

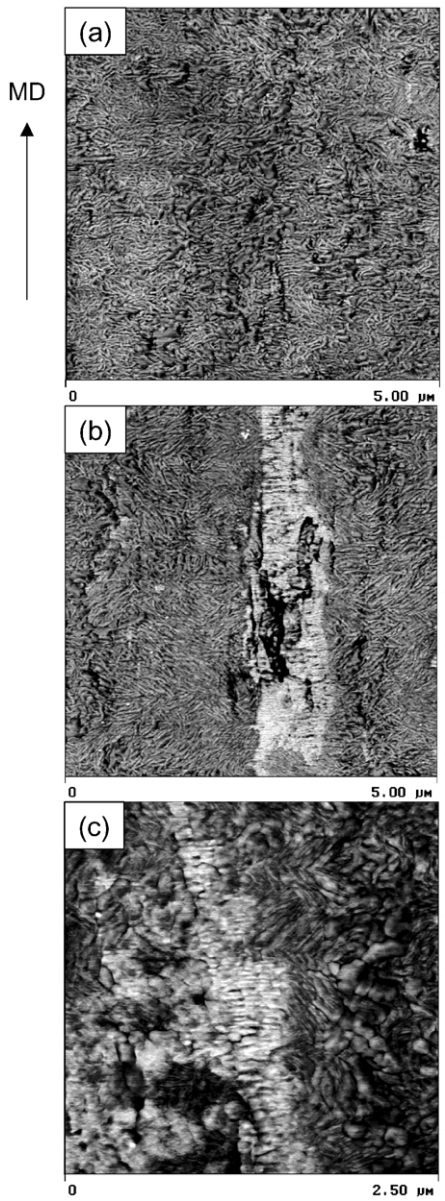

Fig. 9. AFM phase images of 20 μm 10/90 hmsPP/znPE blown film in the normal direction (ND) after etching, with moderately hard tapping. (a) A region without hmsPP domains, (b) a region containing a hmsPP domain, and (c) higher resolution of the interface between a hmsPP domain and the znPE matrix.

densely packed, curving lamellae (compare Fig. 9(a) with Fig. 5(a)). In this case, preferential orientation with the long axis perpendicular to the MD is noticeable. The moderately hard tapping condition ($\cong 50\%\ A_0$) used to reveal lamellar morphology also differentiates the phases. Fig. 9(b) shows a light-colored hmsPP domain extended in the extrusion direction, and the surrounding znPE matrix. The remains of two EPR particles are visible in the hmsPP domain as darker depressions with granular inclusions. The hmsPP lamellae appear to be stacked in a column with lamellar long axes perpendicular to the extrusion direction, similar to the lamellar arrangement in hmsPP film (compare Fig. 9(b) with Fig. 3(a)). Around the hmsPP domain, the polyethylene lamellae are oriented with long axes $\pm 40-50^\circ$ to the MD. These lamellae produce the herringbone pattern characteristic of polyethylene epitaxially crystallized onto polypropylene [37,38]. Away from the hmsPP domain, nonepitaxially crystallized polyethylene lamellae assume the densely packed, curving appearance of lamellae in znPE film (compare with Fig. 5(a)).

A higher resolution image of a hmsPP domain and the surrounding znPE matrix clearly shows columns of hmsPP lamellae oriented perpendicular to the MD and the znPE lamellae crystallized at the characteristic $\pm 40-50^\circ$ angle of the herringbone texture, Fig. 9(c). The image shows no evidence of the amorphous interfacial layer of low molecular weight, highly branched polyethylene fractions that is thought to prevent epitaxial crystallization of polyethylene in injection molded blends of polyethylene and polypropylene [39].

The WAXD patterns of 20 μm 30/70 hmsPP/znPE film in Fig. 10 resolve the hmsPP reflections. The ND and TD patterns resemble those of the 20 μm hmsPP film (compare Fig. 10(a) and (b) with Fig. 4(a) and (b)). The *hk*0 reflections are located on the equator, which is consistent with lamellae arranged in stacks with long axes perpendicular to the MD as observed in the AFM images. In contrast to hmsPP film, the pattern obtained in the MD does not contain rings of equal intensity, Fig. 10(c). The 040 reflection is on the meridian indicating that the *b*-axis is normal to the plane of the film. Furthermore, the highest 110 intensity near the equator indicates that the *a*-axis is in the plane of the film. Thus, lamellae in the row-nucleated structure are not in an axially symmetric arrangement. Rather, the hmsPP domains

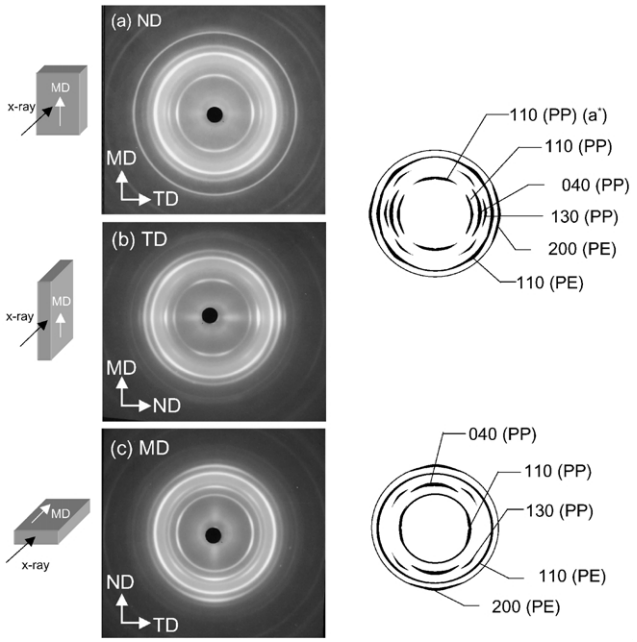

Fig. 10. WAXS patterns from the three orthogonal directions of 20 μm 30/70 hmsPP/znPE blown film showing the hmsPP reflections. (a) ND, (b) TD, and (c) MD.

are thin enough to confine radial growth of lamellae primarily to the plane of the ribbon-shaped domain.

Similar planar shish–kebabs are described in other instances where crystallization from the melt stream is forced to occur in a confined space. Nanolayers of polyethylene or polypropylene, obtained by layer-multiplying coextrusion with polystyrene, have layer thicknesses on a size scale comparable to the molecular dimensions. These conditions produce row-nucleated morphologies of rod-like lamellae [40,41]. By discouraging relaxation of extended chains and enhancing the possibility for fibrous crystals, confinement of the melt stream to the nanoscale produces oriented lamellar growth under process conditions that would not otherwise lead to highly oriented morphologies. This may be a general phenomenon.

The planar shish–kebab morphology of the elongated hmsPP domains, together with the epitaxially crystallized polyethylene, is shown schematically in Fig. 11. Indeed, the hmsPP domains is not much thicker than the lamellae, leading to the conclusion that lamellar growth occurs predominantly in one direction and the resulting lamellae are more like rods than plates. Row-nucleated hmsPP lamellae provide the template for organized crystallization of polyethylene. With the *b*-axis parallel to the TD, the hmsPP domain surface contains the lamellar *ac*-plane as required for epitaxial growth of polyethylene [38]. A 42° lamellar angle correlates with the near lattice match of the

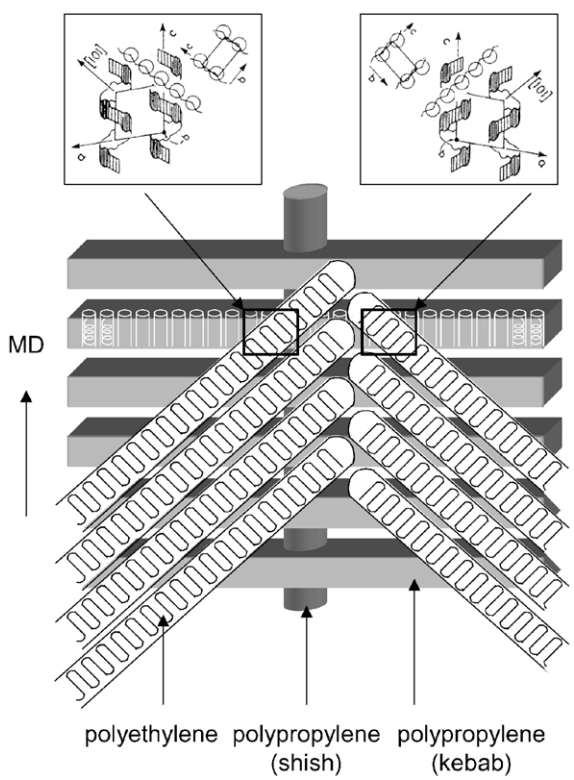

Fig. 11. Schematic representation of polyethylene lamellae epitaxially crystallized on the oriented lamellae of a planar hmsPP shish–kebab in blown film. Insets show the lattice match of polyethylene and polypropylene chains [37].

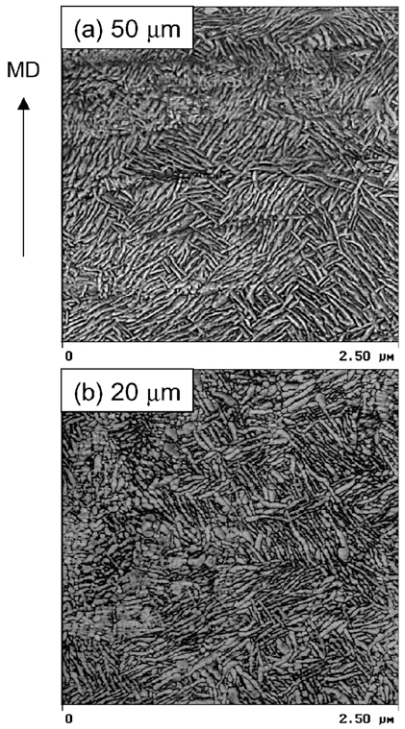

Fig. 12. AFM phase images of 30/70 hmsPP/znPE blown film in the normal direction (ND) after etching, with light tapping. (a) 50 μm film and (b) 20 μm film.

(110) plane of polyethylene with the (010) plane of polypropylene.

Increasing the hmsPP content provides more surface area for epitaxial crystallization. With 30 wt% hmsPP in the blend, most of the znPE matrix in both 50 and 20 μm film exhibits the herringbone texture characteristic of epitaxial crystallization, Fig. 12.

The ND X-ray patterns in Fig. 13 show the znPE reflections. In blend films, the strongest znPE reflections are well-separated from the hmsPP reflections, which occur at smaller diffraction angles. The patterns in Fig. 13 are obtained with a smaller specimen-to-film distance than the pattern in Fig. 10(a) and consequently the main hmsPP reflections of the blend films lie within the bright center ring. In znPE film, 020 reflections reside at the equator as relatively sharp arcs corresponding to preferential orientation of the lamellar long axis perpendicular to the MD, Fig. 13(a). The pattern from the blend film with 10 wt% hmsPP resembles that of znPE film with strong equatorial 020 reflections; however, the 020 reflections also have significant intensity at about ±45° due to the presence of some epitaxially crystallized lamellae. Higher hmsPP content of 20 and 30 wt% produces distinct znPE intensities at approximately ±45° corresponding to the herringbone orientations. The faintness of the remaining equatorial intensity confirms that most of the znPE crystallizes epitaxially. In the MD, the appearance of 020 reflections as equatorial arcs is consistent with planar orientation of the herringbone lamellae. Blends with zn/mPE give the same

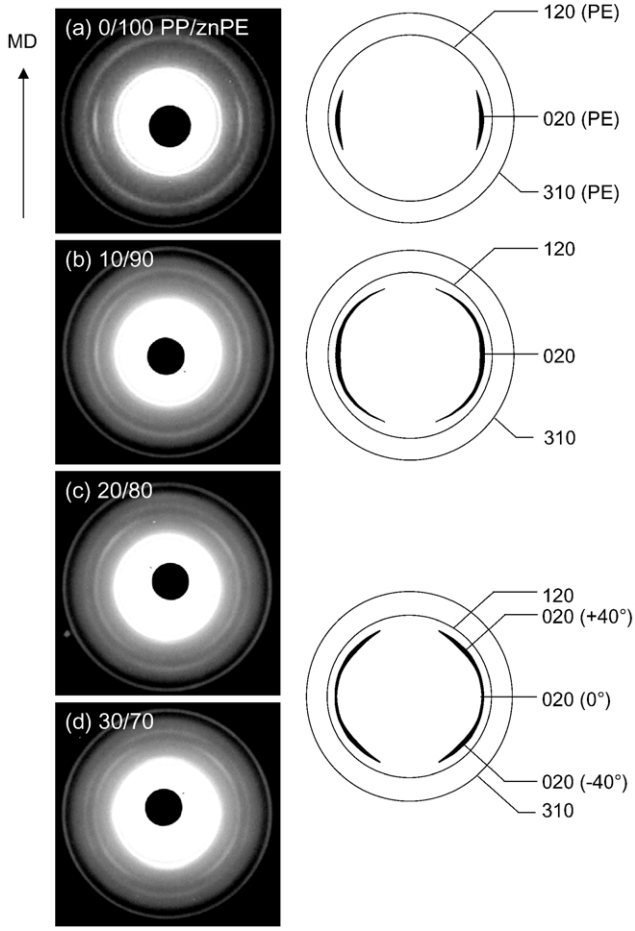

Fig. 13. WAXS patterns from the ND of 20 μm blown film showing the znPE reflections. (a) znPE film, (b) 10/90 hmsPP/znPE, (c) 20/80 hmsPP/znPE, and (d) 30/70 hmsPP/znPE.

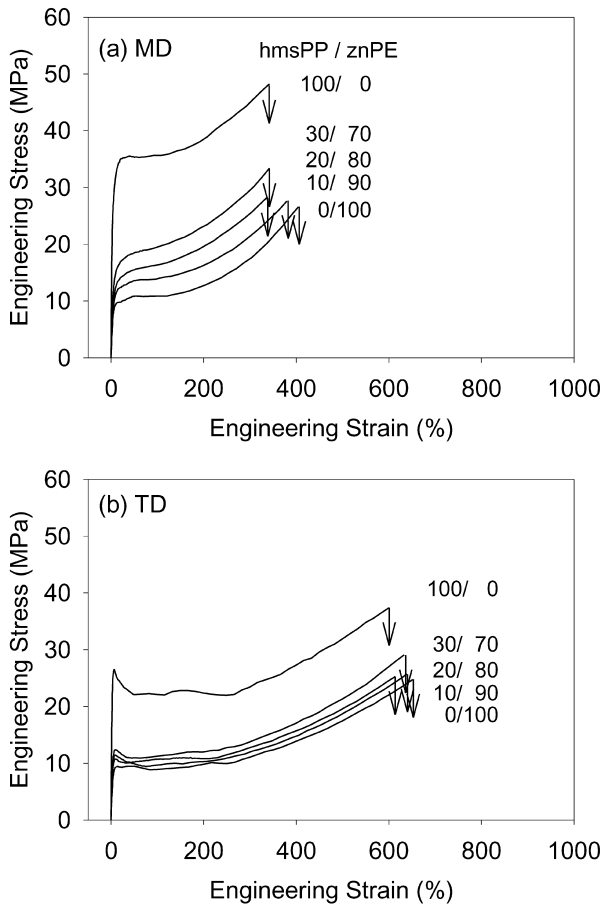

Fig. 14. Effect of blend composition on the stress–strain curve of 20 μm hmsPP/znPE blown film. (a) MD and (b) TD.

results, however, broader reflections from 50 μm film compared to 20 μm film suggest that the epitaxial crystallization is not as well organized.

3.6. Stress–strain behavior

The mechanical response of the films was measured in the MD and TD. The MD stress–strain curve of 20 μm hmsPP is characterized by an initial high slope, followed by a plateau with gradually increasing stress until fracture, Fig. 14(a). Intersection of the initial region of high slope with the plateau region is taken as the yield point, Table 2. Macroscopically, the specimen deforms uniformly up to fracture. Stress-whitening occurs along the entire gauge length just prior to yielding and increases in intensity at higher strains.

The MD stress–strain curve of 20 μm znPE film is described by an initial region of lower modulus than hmsPP, followed by the double change in slope that is characteristic of yielding in linear low density polyethylene. The second slope change, shown to correspond to permanent plastic deformation [42], is taken as the yield point. No macroscopic necking is observed. After the yield point, the entire gauge section deforms uniformly with gradually increasing stress until fracture. Faint stress-whitening occurs just prior to fracture.

The hmsPP/znPE blends have MD stress–strain curves intermediate between those of hmsPP and znPE. Deformation of the blend films is macroscopically uniform. Stress-whitening is faint and increases slightly with hmsPP content. The level of stress response increases approximately proportionally with the hmsPP content, Table 2. Additivity in the mechanical properties indicates that the hmsPP phase is load-bearing. Reinforcement by the hmsPP phase in the MD results from good adhesion to the epitaxially crystallized znPE matrix and orientation of the elongated hmsPP domains with the long axis in the loading direction.

In contrast to the MD stress–strain curve, the TD stress–strain curve of the hmsPP film is characterized by a sharp stress maximum accompanied by stress-whitening and formation of a nearly horizontal shear band, Fig. 14(b). The neck stabilizes as the load drops; subsequent neck propagation corresponds to the plateau portion of the stress–strain curve. An increase in stress accompanies the onset of uniform strain-hardening at about 250% strain. Generally, the stress response after yielding is about 40%

Table 2
Summary of mechanical properties of films

System	PP/PE	Blown film thickness (μm)	2% Secant modulus (MPa)		Yield stress (MPa)		Fracture strain (%)	
			MD	TD	MD	TD	MD	TD
hmsPP/znPE	0/100	50	220 ± 10	260 ± 10	10.6 ± 0.4	10.5 ± 0.2	630 ± 80	650 ± 20
		20	223 ± 7	230 ± 30	11.1 ± 0.3	9.6 ± 0.3	420 ± 30	570 ± 90
	10/90	50	280 ± 30	270 ± 30	12.2 ± 0.3	10.4 ± 0.6	580 ± 30	700 ± 100
		20	250 ± 20	270 ± 26	13.1 ± 0.4	10.4 ± 0.9	380 ± 10	570 ± 100
	20/80	50	310 ± 40	335 ± 5	13.5 ± 0.2	12.0 ± 0.2	540 ± 30	690 ± 30
		20	300 ± 20	350 ± 30	17 ± 1	12.1 ± 0.9	360 ± 30	640 ± 70
	30/70	50	420 ± 20	370 ± 20	16.0 ± 0.3	13.5 ± 0.6	540 ± 50	640 ± 50
		20	360 ± 20	380 ± 20	19.3 ± 0.5	12.8 ± 0.5	340 ± 30	650 ± 40
hmsPP/zn/mPE	0/100	50	181 ± 7	210 ± 10	10.0 ± 0.2	9.4 ± 0.2	560 ± 40	610 ± 80
		20	160 ± 6	160 ± 22	11.3 ± 0.7	8.8 ± 0.1	400 ± 10	540 ± 60
	10/90	50	250 ± 10	270 ± 20	11.5 ± 0.1	10.0 ± 0.3	540 ± 40	600 ± 20
		20	220 ± 20	240 ± 30	13.8 ± 0.8	9.7 ± 0.3	350 ± 20	610 ± 40
	20/80	50	330 ± 20	300 ± 20	13.4 ± 0.5	11.2 ± 0.4	490 ± 20	610 ± 50
		20	260 ± 17	280 ± 40	16.3 ± 0.7	10.7 ± 0.4	350 ± 20	620 ± 30
	30/70	50	390 ± 7	350 ± 20	15.9 ± 0.5	12.8 ± 0.2	440 ± 90	640 ± 50
		20	320 ± 20	328 ± 7	18 ± 1	11.7 ± 0.3	320 ± 40	590 ± 90
	100/0	50	970 ± 60	870 ± 40	30.6 ± 0.6	25.9 ± 0.4	440 ± 90	640 ± 50
		20	1060 ± 40	930 ± 80	37 ± 1	25.1 ± 0.9	330 ± 20	570 ± 70

lower in the TD than in the MD. However, the TD is more ductile exhibiting nearly twice the fracture strain of the MD. The anisotropic mechanical response of hmsPP film results from the oriented stacked lamellar structure (Fig. 3).

The TD stress–strain curve of znPE film exhibits a double yield with about the same yield stress as in the MD; however, a diffuse neck accompanies yielding in the TD. Strain-hardening is more gradual and the fracture strain is higher in the TD than in the MD. The stress–strain response of znPE film is much more closely balanced in the MD and TD directions than the response of hmsPP film. This is consistent with the relatively irregular organization of znPE lamellae compared to the highly oriented lamellar morphology of hmsPP film (compare Fig. 3 with Fig. 5(a)).

In the TD, the blend films exhibit stress–strain behavior that is nearly identical to that of znPE film. Increasing hmsPP content results in only slightly higher stress response and a slightly sharper neck. Stress-whitening is minimal. The weak compositional effect results from the anisotropic domain morphology. Orientation of the elongated hmsPP domains perpendicular to the loading direction provides minimal reinforcement. As a consequence, the TD response of the blend films closely resembles that of the matrix.

The 2% secant modulus, yield stress, and fracture strain of 20 and 50 μm films of znPE and zn/mPE blended with hmsPP are summarized in Table 2. There are no significant differences between hmsPP/znPE blends and hmsPP/(zn/mPE) blends in uniaxial tension. In general, hmsPP increases the modulus of blown film approximately in proportion to the composition. Thus, blending with 30 wt% hmsPP approximately doubles the modulus and yield stress of polyethylene film.

The effect of greater anisotropy of the hmsPP domains in 20 μm film compared to 50 μm film is evident in the yield stress and the elongation at fracture. The MD yield stress is significantly higher in 20 μm film than in 50 μm film. In the TD, the yield stress is slightly lower in 20 μm film. As a consequence, the yielding characteristics are more balanced in the thicker film. Similarly, the MD elongation at fracture is significantly lower in 20 μm film than in 50 μm film. These differences are consistent with the higher aspect ratio (length-to-width) of the hmsPP ribbons in 20 μm film compared to the planks in 50 μm film (Fig. 8).

4. Conclusions

This study examines the hierarchical structure of blown film processed from linear low density polyethylene blended with up to 30 wt% of a hmsPP. Good compatibility of the blend constituents results in a fine dispersion of elongated hmsPP domains in the polyethylene matrix. The crystallizable EPR component remains in the hmsPP phase; however, the amorphous EPR fractions may be mobile and able to redistribute. Within domains, hmsPP crystallizes as row-nucleated structures with lamellae oriented perpendicular to the extrusion direction. The hmsPP domains are thin enough to confine radial growth of lamellae primarily to the plane of the elongated domain. Indeed, the resulting lamellae are more like rods than plates. They resemble other planar row-nucleated structures where crystallization from the melt stream is forced to occur in a confined space. Row-nucleated hmsPP lamellae provide a template for epitaxial crystallization of polyethylene lamellae. The 42° angle of

the lattice match imparts a characteristic herringbone texture to the polyethylene. The hmsPP phase reinforces the tensile modulus and strength of polyethylene film to a degree consistent with the domain morphology without significantly affecting the ultimate elongation.

Acknowledgments

The technical and financial support of The Dow Chemical Company is gratefully acknowledged.

References

[1] Benning CJ. Plastic films for packaging. Landcaster: Technomic; 1983. p. 37–43.
[2] Scheve BJ, Mayfield JW, DeNicola Jr AJ. US Patent 3,637,458; 1972.
[3] Yu DW, Dey SK, Pringgosusanto F, Xanthos M. Proc SPE ANTEC 2000;1847–50.
[4] Khan SA, Prud'homme RK, Larson RG. Rheol Acta 1987;26:144–51.
[5] Larson RG, Khan SA, Raju VR. J Rheol 1988;32:145–61.
[6] Hoenig WD, Bosnyak CP, Sehanobish K, Van Volkenburgh W, Ruiz C, Tau LM. Proc SPE ANTEC 2000;1843–6.
[7] Wu S, Bosnyak C, Faul D, Tau L, Huang Y. Proc SPE ANTEC 2001; 2828–32.
[8] Lee IH, Schultz JM. J Mater Sci 1988;23:4237–43.
[9] Petermann J, Broza G, Rieck U, Kawaguchi A. J Mater Sci 1987;22: 1477–81.
[10] Gross B, Petermann J. J Mater Sci 1984;19:1105–12.
[11] Jaballah A, Rieck U, Petermann J. J Mater Sci 1990;25:3105–10.
[12] Olley RH, Bassett DC. Polymer 1982;23:1707–10.
[13] Kolbert AC, Didier JG. J Appl Polym Sci 1999;71:523–30.
[14] Lehtinen A, Paukkeri R. Macromol Chem Phys 1994;195:1539–56.
[15] Hongjun C, Xiaolie L, Dezhu M, Jiamin W, Hongsheng T. J Appl Polym Sci 1999;74:93–101.
[16] Zacur R, Goizueta G, Capiati N. Polym Engng Sci 2000;40:1921–30.
[17] D'Orazio L, Mancarella C, Martuscelli E, Cecchin G, Corrieri R. Polymer 1999;40:2745–57.
[18] Yoshii F, Makuuchi K, Kikukawa S, Tanaka T, Saitoh J, Koyama K. J Appl Polym Sci 1996;60:617–23.
[19] Sugimoto M, Tanaka T, Masubuchi Y, Takimoto J, Koyama K. J Appl Polym Sci 1999;73:1493–500.
[20] Sugimoto M, Masubuchi Y, Takimoto J, Koyama K. Macromolecules 2001;34:6056–63.
[21] Binsbergen FL, de Lange BGM. Polymer 1968;9:23–40.
[22] Norton DR, Keller A. Polymer 1985;26:704–16.
[23] Padden FJ, Keith HD. J Appl Phys 1966;37:4013–20.
[24] Lindenmeyer PH, Lustip S. J Appl Polym Sci 1965;9:227–40.
[25] Nie HY, Walzak MJ, McIntyre NS. Polymer 2000;41:2213–8.
[26] Keller A, Machin MJ. J Macromol Sci Phys 1967;B1:41–91.
[27] Odell JA, Grubb DT, Keller A. Polymer 1978;19:617–26.
[28] Zhou H, Wilkes GL. J Mater Sci 1998;33:287–303.
[29] Ratta V, Wilkes GL, Su TK. Polymer 2001;42:9059–71.
[30] Mencik Z, Fitchmun DR. J Polym Sci: Polym Phys Ed 1973;11: 973–89.
[31] Fujiyama M, Wakino T, Kawasaki Y. J Appl Polym Sci 1988;35: 29–49.
[32] Bunn CW. Trans Faraday Soc 1939;35:482–91.
[33] Turner-Jones A, Cobbold AJ. J Polym Sci 1968;B6:539–46.
[34] Kavesh S, Schultz JM. J Polym Sci, Part A-2 1970;8:243–76.
[35] Qureshi NZ, Stepanov EV, Capaccio G, Hiltner A, Baer E. Macromolecules 2001;34:1358–64.
[36] Qureshi NZ, Rogunova M, Stepanov EV, Capaccio G, Hiltner A, Baer E. Macromolecules 2001;34:3007–17.
[37] Lotz B, Wittman JC. J Polym Sci, Part B: Polym Phys 1987;25: 1079–87.
[38] Wittman JC, Lotz B. Prog Polym Sci 1990;15:909–48.
[39] Chaffin KA, Bates FS, Brant P, Brown GM. J Polym Sci, Part B: Polym Phys 2000;38:108–21.
[40] Pan SJ, Hill MJ, Keller A, Hiltner A, Baer E. J Polym Sci, Part B: Polym Phys 1990;28:1105–19.
[41] Rogunova M, Hiltner A, Baer E, Nowacki R, Galeski A, Piorkowska E. Unpublished results.
[42] Brooks NW, Duckett RA, Ward IM. Polymer 1992;33:1872–80.